BIOCHEMISTRY

 Volume 44, Number 20 May 24, 2005

Accelerated Publications

Design of a Redox-Linked Active Metal Site: Manganese Bound to Bacterial Reaction Centers at a Site Resembling That of Photosystem II[†,‡]

M. Thielges, G. Uyeda, A. Cámara-Artigas,[§] L. Kálmán,[||] J. C. Williams, and J. P. Allen*

Department of Chemistry and Biochemistry, Arizona State University, Tempe, Arizona 85287

Received February 28, 2005; Revised Manuscript Received April 7, 2005

ABSTRACT: Metals bound to proteins perform a number of crucial biological reactions, including the oxidation of water by a manganese cluster in photosystem II. Although evolutionarily related to photosystem II, bacterial reaction centers lack both a strong oxidant and a manganese cluster for mediating the multielectron and proton transfer needed for water oxidation. In this study, carboxylate residues were introduced by mutagenesis into highly oxidizing reaction centers at a site homologous to the manganese-binding site of photosystem II. In the presence of manganese, light-minus-dark difference optical spectra of reaction centers from the mutants showed a lack of the oxidized bacteriochlorophyll dimer, while the reduced primary quinone was still present, demonstrating that manganese was serving as a secondary electron donor. On the basis of these steady-state optical measurements, the mutant with the highest-affinity site had a dissociation constant of approximately 1 μM. For the highest-affinity mutant, a first-order rate with a lifetime of 12 ms was observed for the reduction of the oxidized bacteriochlorophyll dimer by the bound manganese upon exposure to light. The dependence of the amplitude of this component on manganese concentration yielded a dissociation constant of approximately 1 μM, similar to that observed in the steady-state measurements. The three-dimensional structure determined by X-ray diffraction of the mutant with the high-affinity site showed that the binding site contains a single bound manganese ion, three carboxylate groups (including two groups introduced by mutagenesis), a histidine residue, and a bound water molecule. These reaction centers illustrate the successful design of a redox active metal center in a protein complex.

Pigment−protein complexes convert light energy into chemical energy in photosynthetic organisms. In purple anoxygenic bacteria, reaction centers embedded in the membrane perform light-driven charge separation (*1*). The primary electron donor of the reaction center from *Rhodobacter sphaeroides* is a bacteriochlorophyll *a* dimer (P)[1] which upon excitation becomes oxidized through electron

[†] This work was supported by Grant MCB 0131764 from the National Science Foundation.

[‡] The coordinates and structure factors for the structures reported here are available from the Protein Data Bank (entries 1Z9K and 1Z9J for the wild type and mutant, respectively).

* To whom correspondence should be addressed. Phone: (480) 965-8241. Fax: (480) 965-2747. E-mail: jallen@asu.edu.

[§] Permanent address: Departamento de Química Física, Bioquímica y Química Inorgánica, Universidad de Almería, Almería, Spain.

[||] Permanent address: Department of Biophysics, University of Szeged, Egyetem u.2, H-6722 Szeged, Hungary.

[1] Abbreviations: P, bacteriochlorophyll dimer; EPR, electron paramagnetic resonance; M1, mutant with high-potential changes and Glu introduced at M168 and M192; M2, mutant with high-potential changes and Glu introduced at M168 and Asp at M288; M3, mutant with high-potential changes and Glu introduced at M192 and Asp at M288; M4, mutant with high-potential changes and Glu introduced at L168 and M192 and Asp at M288; Q_A^-, reduced primary quinone.

10.1021/bi050377n CCC: $30.25
Published on Web 04/26/2005

transfer to a quinone via intermediate cofactors. The oxidation−reduction midpoint potential of the P/P^+ couple can be altered by modifications of the hydrogen bonding pattern of P with nearby amino acid residues (*2*). This plasticity in the midpoint potential expands the range of redox chemistry that P can undergo, and modification by multiple mutations that increase the P/P^+ midpoint potential enables the oxidation of specific tyrosine residues (*3*). Manganese can also be oxidized by modified reaction centers, but only weak binding of manganese to the reaction center, with a dissociation constant of >100 μM and a second-order rate constant for manganese oxidation, was observed (*4*). In this work, a manganese-binding site was designed in reaction centers such that the tightly bound manganese could donate an electron to P^+.

Protein engineering of novel metal centers that can carry out specific reactions is a challenging area of rational structure-based design (*5*). Designs for a manganese cofactor that would serve as a secondary electron donor to P^+ were constrained by consideration of both the coordination of the manganese and the location of the binding site near P. Manganese in proteins is typically coordinated in an approximate octahedral geometry by two to four aspartate, glutamate, or histidine residues (*6*). In photosystem II, the manganese cluster is assembled through a light-dependent process called photoactivation (*7*). The first step of this process involves the binding of a single manganese(II) ion to a high-affinity binding site, and carboxylate residues, in particular, Asp 170 of the D1 subunit, have been shown to be required for this binding (*8*, *9*). Although photosystem II is more complex, the core D1 and D2 subunits are homologous in structure and sequence to the L and M subunits of the bacterial reaction center (*10*−*12*). The residue Glu M173 in the reaction center from *R. sphaeroides* is in the position corresponding to Asp D1-170 (*11*), and this residue was included as a ligand to manganese in all designs for the manganese-binding sites. This location places the metal site approximately 10 Å from P. At this distance, the manganese ligands are sufficiently far from P that they would not involve changes in any amino acid residues in contact with P while being sufficiently close to allow efficient electron transfer from the bound Mn^{2+} to P^+. In addition, M173 is near the surface of the reaction center in a region that would be more accommodating to the incorporation of the manganese and ligands than a buried interior site. In this paper, mutants with different designs for manganese-binding sites generated by modeling carboxylate residues near Glu M173 are characterized by determination of the binding affinity for Mn^{2+}, the ability of Mn^{2+} to transfer an electron to P^+, and the three-dimensional structure.

METHODS

Design of Mutants. Potential manganese-binding sites in the reaction center were generated by modeling carboxylate residues in the wild-type structure using Insight II (Biosym/MSI). Amino acid residues near Glu M173 were replaced with aspartate or glutamate to identify a set that could ligate manganese in approximate octahedral coordination. The oxygen atoms of the carboxyl residues were positioned by rotation of the $C_\beta-C_\gamma$ bond of aspartate or the $C_\gamma-C_\delta$ bond of glutamate residues, using different rotamer orientations of the side chains. Residues involved in interactions with P were avoided to minimize perturbation of its redox properties. The substitution of Tyr for Arg at M164 was also included in all of the mutants, as this change removes the salt bridge interaction between Arg M164 and Glu M173 found in the wild type and also makes the region more similar to photosystem II, where Tyr D1-161 at the analogous location is active in the electron-transfer reactions associated with water oxidation.

Three substitutions, Met M168 to Glu, Val M192 to Glu, and Gly M288 to Asp, were found to yield appropriate designs. Four variations of the binding site were created by different combinations of these mutations. In each of the computer-generated models, the distance from the manganese to the oxygen of the residues was between 2.1 and 2.8 Å. These distances are in the range observed for manganese-binding proteins, indicating that manganese coordination would be feasible.

Mutant Construction and Protein Isolation. Mutants were constructed by oligonucleotide-directed mutagenesis and manipulation of restriction fragments (*2*, *13*, *14*). The M1 mutant contains the Met M168 to Glu and Val M192 to Glu changes. The M2 mutant contains the Met M168 to Glu and Gly M288 to Asp changes. The M3 mutant contains the Val M192 to Glu and Gly M288 to Asp changes. The M4 mutant contains the Met M168 to Glu, Val M192 to Glu, and Gly M288 to Asp changes. The M1−M4 mutants and the control mutant all contain the Leu L131 to His, Leu M160 to His, and Phe M197 to His changes, used to increase the P/P^+ midpoint potential, and the Arg M164 to Tyr mutation, which incorporates a tyrosine residue near P (*3*). The altered genes were introduced into *R. sphaeroides* deletion strain ΔLM1.1 (*15*). The strains were grown semiaerobically in the dark for 3−4 days at 30 °C. For X-ray diffraction measurements, the reaction centers were isolated using published protocols (*13*) with the purified protein dialyzed against 15 mM Tris-HCl (pH 8) and 0.025% lauryl dimethylamine oxide before crystallization. For spectroscopic measurements, after solubilization, the reaction centers were purified using ion exchange chromatography with DEAE-Sephacryl equilibrated with 0.05% Triton X-100 instead of 0.1% lauryl dimethylamine oxide. After the chromatography, the reaction centers were dialyzed against 15 mM Tris-HCl (pH 8) and 0.05% Triton X-100 to remove EDTA.

Steady-State and Transient Optical Spectroscopy. The fraction of reaction centers containing bound manganese in the presence of 0−1 mM $MnCl_2$ was monitored by measuring the light-induced changes in the absorption spectrum from 700 to 1000 nm in a Cary 5 spectrophotometer (Varian). An Oriel tungsten lamp with an 860 ± 15 nm interference filter was used to illuminate the samples. The intensity was adjusted to approximately one-third of the saturating value of the wild type. For this intensity, the spectra were relatively insensitive to increases in illumination intensity and duration by a factor of 2. Before all titrations, the reaction centers were diluted in 15 mM CHES and 0.05% Triton X-100 (pH 8.9−9.4) to a concentration of 0.4−1.5 μM with 100 μM terbutryne to block electron transfer to the secondary quinone.

The dissociation constant of manganese II binding to the reaction center was determined using a metal binding analysis previously described (*16*). The fraction of reaction centers

with bound metal (R_M), can be expressed in terms of the dissociation constant of manganese II binding (K_D), the concentration of added manganese II ([Mn]), and the total concentration of reaction centers ([RC]) as

$$R_M = \frac{[Mn] + [RC] + K_D - \sqrt{([Mn] + [RC] + K_D)^2 - 4[RC][Mn]}}{2[RC]} \quad (1)$$

The fraction of reaction centers bound by manganese was found by monitoring the bleaching of the P band at 865 nm. Assuming the complete oxidation of manganese bound to reaction centers, the fraction of reaction centers without bound metal is given by the relative bleaching at 865 nm for reaction centers with manganese (ΔA_M^{865}) and in the absence of manganese (ΔA_0^{865}):

$$\frac{\Delta A_M^{865}}{\Delta A_0^{865}} = 1 - R_M \quad (2)$$

The recovery of the primary donor after a single saturating flash was measured with a single-beam spectrometer of local design (*17*). A ND:YAG (Continuum) laser with a 5 ns laser pulse was used to excite the reaction centers at 532 nm, and the transient change in absorption at 865 nm was monitored. The transient optical measurements were performed in 15 mM Tris (pH 8), 0.05% Triton X-100, and 100 μM terbutryne. The recoveries were fit to one or two exponentials using a nonlinear least-squares method. The amplitude of the slow kinetic component (A_{slow}) compared to the total amplitude (A_{total}) was used to calculate the fraction of reaction centers without bound metal:

$$\frac{A_{slow}}{A_{total}} = 1 - R_M \quad (3)$$

Protein Crystallography. Reaction centers from the wild-type and M2 strains were crystallized following conditions similar to those previously described (*18*) except for the substitution of manganese chloride for sodium chloride. Using vapor diffusion, a protein solution containing 12% polyethylene glycol 4000, 3.9% heptane triol, 0.06% lauryl dimethylamine oxide, 200 mM manganese chloride, 0.04 M sodium chloride, and reaction centers at a concentration A^{802} of 25 was equilibrated with a reservoir containing 15% polyethylene glycol 4000. Crystals could be grown without sodium chloride but grew to their largest size of approximately 0.3 mm × 0.3 mm × 0.5 mm when 10−40 mM sodium chloride was included. A detailed description of the crystallization of the wild type will be published elsewhere.

These crystals belong to a tetragonal form, $P4_222$, not previously described for reaction center crystals. X-ray diffraction data were measured for both the wild type and the M2 mutant using a RAXIS IV detector mounted on a rotating anode with Osmic mirrors. The diffraction measurements were processed using Mosflm (*19*) to resolution limits of 4.6 and 4.5 Å for the wild type and the M2 mutant, respectively. Using a wild-type structure (*20*), the position of the reaction center in the $P4_222$ cell was readily found and refined using CCP4 (*21*) and CNS (*22*).

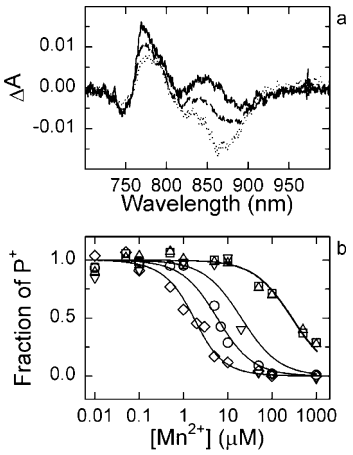

FIGURE 1: Manganese binding measurements of the different mutants at pH 9. (a) Changes in the light-minus-dark difference optical spectra of the M4 mutant in the presence of 0 (dotted line), 7 (dashed line), and 50 μM (solid line) $MnCl_2$ indicate reduction of P^+ by manganese. (b) Representative manganese binding curves fit using eq 2 with dissociation constants of 1.0, 5.0, and 19.7 μM for the M2 (◇), M1 (○), and M4 (▽) mutants, respectively. The M3 mutant (△) had a dissociation constant of >100 μM that was indistinguishable from that of the control mutant (□), which contained none of the changes for manganese binding but did have alterations, common to all of the mutants, that result in a highly oxidizing P.

RESULTS

Characterization of Manganese Oxidation in the Mutant Reaction Centers by Optical Spectroscopy. In the absence of manganese, the light-induced spectra of the mutants were similar to those of the wild type (Figure 1), exhibiting features characteristic of both P^+ and the reduced primary quinone (Q_A^-). The features associated with P^+ are an absorption decrease near 865 nm, an electrochromic shift of the bacteriochlorophyll monomer near 800 nm, and an electrochromic shift near 770 nm arising from the presence of a negative charge on Q_A^-. As the manganese concentration was increased, the magnitude of the absorption change at 865 nm correspondingly decreased due to the loss of P^+. In all cases, the amplitude of the spectral features of Q_A^- slightly increased as the amount of manganese increased, presumably due to a longer lifetime of the $Mn^{3+}PQ_A^-$ state (Figure 1). At high concentrations of Mn^{2+}, the features associated with P^+ were no longer present with only the features associated with Q_A^- remaining, including a small electrochromic shift of the 865 nm band. Within approximately 5 min of the end of illumination, these spectral features were no longer present, indicating that the reaction centers had fully recovered.

The fraction of reaction centers with bound manganese, determined by the relative amount of P^+ reduced in the presence of manganese, was found to systematically increase with an increase in Mn^{2+} concentration (Figure 1). Fitting these data to eq 2 yielded a dissociation constant for each mutant. The mutants showed different binding affinities, with M2 having a tight binding site, M1 and M4 having comparable and weaker binding sites, and M3 being unchanged relative to the control strain. On the basis of multiple

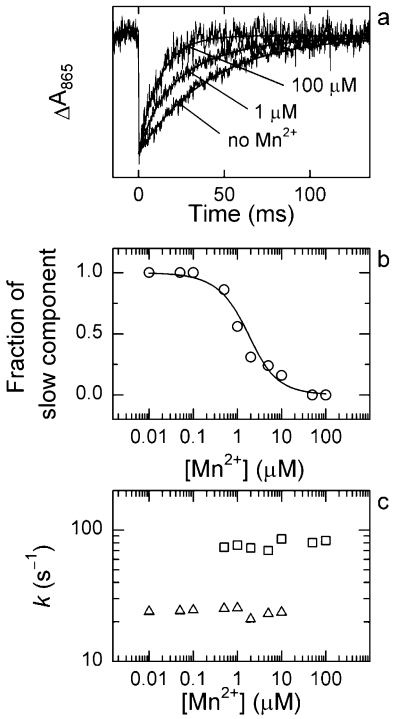

FIGURE 2: Kinetics of P^+ reduction in the M2 mutant at pH 9. (a) The decay rate of P^+, as measured by the change in absorption at 865 nm, significantly increased in the presence of Mn^{2+} compared to the rate in the absence of Mn^{2+}. The lines are fits showing that P^+ recovered with a lifetime of 42 ms with no Mn^{2+}, the decay was biphasic with a slow and a fast component with 1 μM Mn^{2+}, and only the fast component with a lifetime of 12 ms was observed with 100 μM Mn^{2+}. (b) The relative fraction of the slow component decreased with the amount of Mn^{2+}. The solid line is a fit of the data using eq 3 with a dissociation constant of 1.0 μM. (c) The rates of both the fast and slow components were independent of the amount of Mn^{2+}, with measured rates of 74−83 s^{-1} (lifetimes of 12−14 ms) for reduction of P^+ by bound Mn^{2+} (□) and 21−26 s^{-1} (lifetimes of 39−48 ms) for reduction of P^+ by charge recombination from Q_A^- (△).

measurements, dissociation constants of 1.5 ± 1, 8 ± 3, and 14 ± 5 μM for the M2, M1, and M4 mutants, respectively, were obtained.

In kinetic measurements, the recovery of P^+ at 865 nm became faster when Mn^{2+} was added (Figure 2). For the M2 mutant, the $P^+Q_A^-$ charge recombination time was 42 ms in the absence of manganese. When manganese was present, the recovery was biphasic and could be fitted by including a second exponential term with a lifetime of approximately 12 ms. The rate of this fast component was independent of the manganese concentration, showing that it arose from a first-order reaction, and it is assigned to reduction of P^+ by the bound manganese. The rate of charge recombination, as determined from the slower component, was also found to be independent of manganese concentration. As the manganese concentration was increased, the relative amplitude of the slow component decreased compared to that of the fast component. The dependence of these components on the manganese concentration provided an independent measure of the manganese binding affinity. The fraction of the slow component was fitted to eq 3, yielding a dissociation constant of approximately 1 μM, similar to the value of the dissociation constant determined from the steady-state measurements. The observed rate of P^+ recovery was much faster than the rates associated with tyrosine oxidation in modified reaction centers (*3*, *23*), and there was no evidence that Tyr M164 plays a role in metal oxidation under these conditions.

The M1 and M4 mutants also showed an increase in the observed recovery rate in the presence of manganese, but no change was evident for the M3 or control mutant, even when the manganese concentration was 100 μM (data not shown). The lack of any change for the control mutant shows that the rate of electron transfer from exogenous manganese is much slower than the $P^+Q_A^-$ charge recombination rate. Thus, this second-order process does not contribute to the observed spectral decreases at 1−10 μM manganese in the steady-state absorption measurements, and is only evident at higher manganese concentrations.

Determination of Structural Changes Associated with the Mutations and Manganese Binding by Protein Crystallography. When manganese(II) chloride was substituted for sodium chloride in crystallization conditions that have previously resulted in an orthorhombic form (*18*), reaction centers from both the wild type and the M2 mutant crystallized in a tetragonal form that diffracted to a resolution limit of approximately 4.5 Å. The resulting structures of the wild type and the M2 mutant were very similar, with the only notable region of difference being at the mutation site, which showed a significant amount of electron density in the M2 mutant but not in the wild type (Figure 3). While the basic features of the manganese binding have been identified in the mutant, the limited resolution does not allow detailed modeling of bond distances and angles. The electron density for the M2 mutant at the site of the mutations had one prominent peak assigned to manganese and an extended region that is modeled as arising from the presence of two water molecules. After incorporation of the amino acid changes and the manganese atom, the resulting structural model refined to an *R*-factor of 30% and an R_{free} of 34%. This structure of the M2 mutant is in agreement with the initial design as Glu M173, Glu M168, and Asp M288 are clearly in the binding site (Figure 3). The manganese and residues Asp M288 and Asp M292 interact with the bound water molecules. These residues are located in a C-terminal loop region, which is shifted in the mutant approximately 0.5 Å relative to that in the wild type. Also nearby is His M193, a putative proton acceptor for Tyr M164 in a different highly oxidizing reaction center (*3*). The three-dimensional structure shows that the imidazole ring of His M193 shifts in position compared to that of the wild type and provides a ligand opposite to Glu M168.

DISCUSSION

A manganese center has been introduced into modified reaction centers at a distance of approximately 13 Å from the conjugated system of P, and the manganese efficiently transfers an electron to P with a lifetime of 12 ms. This new electron-transfer reaction is consistent with the observation that rapid electron transfer in proteins occurs at distances of <14 Å even when parameters such as the free energy difference and reorganization energy are not optimized (*24*). For the M2 mutant, the manganese binds tightly with a dissociation constant of 1 μM determined from two independent measurements. The manganese bound less tightly to the M1 and M4 mutants, while no change in manganese binding was evident for the M3 mutant compared to the

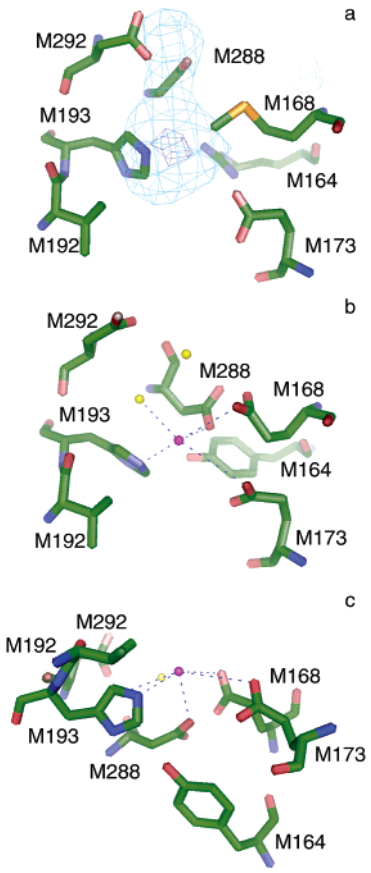

FIGURE 3: Structural evidence for Mn binding. (a) The highest peak in the electron density $F_o - F_c$ difference map using the coordinates of the wild-type reaction center and the observed structure factors of the M2 mutant is at this location with strong electron density evident at 6.5σ (dark blue) and a more elongated electron density at 3.0σ (light blue). (b and c) Two perpendicular views of the structure of the M2 mutant showing the manganese(II) ion (purple sphere) and the closest nearby residues Glu M168, Glu M173, His M193, and Asp M288. Also shown are two bound water molecules (yellow spheres) and Tyr M164, Val M192, and Glu M292.

control. The presence of manganese at the designed site was verified by the determination of the three-dimensional structure of the M2 mutant using protein crystallography.

The measured binding affinity for manganese clearly differs for the four different mutants, although the original computer designs showed a similar modeling of the coordination of manganese. Comparison of the relative affinities and designs of the mutants points to particular amino acid residues being key to the binding of manganese at this site. For example, the presence of Glu M168 appears to be critical, as it is found in the three mutants, M1, M2, and M4, that show improved binding relative to the control, but is missing in the M3 mutant that has a dissociation constant indistinguishable from that of the control. The three-dimensional structure of the M2 mutant, which had the highest affinity for manganese, shows that the imidazole ring of His M193 shifts in position compared to that of the wild type and provides a ligand opposite to Glu M168. This pairing of His M93 and Glu M168 across the manganese appears to be significant, and was not modeled in the original design. Part of the reason that Glu M192, which is found in the M1, M3, and M4 mutants but not the M2 mutant, may be less effective in the coordination of manganese is that it is adjacent to His M193 and so would be in an unfavorable position to form a

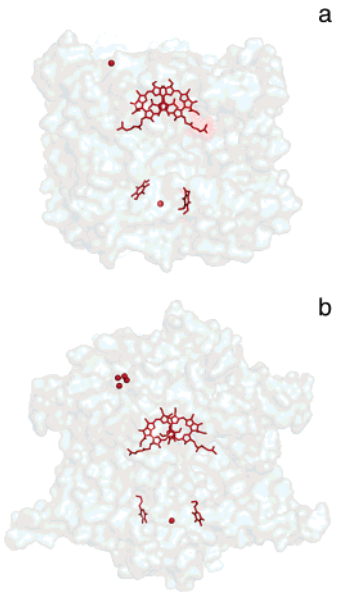

FIGURE 4: Comparison of structural models of the M2 mutant (a) and photosystem II (b). The (bacterio)chlorophylls serving as the primary electron donor, the quinone acceptors, the non-heme iron, and the bound manganese are shown (red), along with surface representations of the L and M subunits of the reaction center and of the D1 and D2 subunits of photosystem II (light gray). The manganese is located in similar positions near the surface of the protein and the primary electron donor. The phytyl and isoprenoid chains have been truncated. Coordinates for the M2 mutant structure are from PDB entry 1Z9J, and coordinates for the photosystem II structure are from PDB entry 1S5L (*25*).

Glu-His pair. Asp M288 was incorporated in the M2, M3, and M4 mutants, and the structure of the M2 mutant shows that it serves both as a ligand and in the stabilization of the two bound water molecules, along with Glu M168 and Glu M292. Glu M292 is part of the C-terminal loop that has shifted in the structure of M2 relative to that of the wild type, and this interaction of Glu M292 with water molecules in the binding site was also not modeled in the original design. The M4 mutant has the Asp M288 residue in addition to the Glu M168 and Glu M192 residues found in the M2 mutant, and the lower affinity for manganese compared to that of the M2 mutant is probably due to the additional negative charge. Thus, while the original design of manganese binding to the introduced carboxylates proved to be successful, the mutants show differences in binding affinities due to the involvement of amino acid residues such as His M193 and Glu M292 near the carboxylates that were not part of the original design.

The manganese-binding site of M2 is similar in a number of ways to the binding site of the four-manganese cluster of photosystem II, including the location on the protein (Figure 4). Several residues near the binding site in the reaction center, including Glu M173, His M193, and Tyr M164, have counterparts in photosystem II, in this case, Asp D1-170, His D1-190, and Tyr D1-161, respectively (*11*, *25*). The designed site has a carboxylate group at a position comparable to Asp D1-170, which is thought to initiate manganese binding in the photoactivation process. In photosystem II, water can be converted to molecular oxygen in part because P680 has a midpoint potential of more than 1 V, whereas P with a midpoint potential of approximately 0.5 V in wild-type bacterial reaction centers is not a sufficiently strong oxidant (*26*). On the basis of the hydrogen bond mutations

used to modify the potential, the P/P^+ midpoint potential of these manganese-binding mutants is estimated to be increased relative to that of the wild type by approximately 0.27 mV (*2*). The mutations at the manganese-binding site are expected to have a small electrostatic effect on the P/P^+ midpoint potential (*27*). Other mutations have been shown to result in an increase in the potential above 0.8 V, which is necessary for water oxidation and provides the capacity to oxidize Tyr M164 (*3*). Thus, this design also provides the opportunity to couple electron transfer to proton transfer and opens the possibility of investigating the mechanism of manganese cofactor incorporation in proteins such as photosystem II.

The development of a bacterial reaction center with bound manganese that serves as an efficient secondary electron donor to P^+ demonstrates that with a limited number of amino acid changes, a primitive photosystem could have achieved both a potential sufficient to oxidize manganese and a manganese-binding site near P. Manganese is found in sediments, and its availability could have provided a manganese-oxidizing primitive photosystem with a special ecological niche. No anoxygenic phototroph has been identified as being capable of manganese oxidation, although a number of photosynthetic bacteria can oxidize iron (*28*).

The design of proteins with new metal cofactors that have well-defined redox activity remains a biochemical challenge (*29*). The incorporation of manganese into the bacterial reaction center provides an opportunity to determine how proteins control the properties of bound metals through the interactions between the metal and nearby amino acid residues. For example, these results provide the basis for investigating the specificity for manganese binding and the factors that control the redox activity of the metal. In addition, since the oxidation state of P is controlled by light, the manganese-binding mutants provide the foundation for the development of a light-driven metal-based catalyst.

SUPPORTING INFORMATION AVAILABLE

Details concerning the crystallographic data collection and analysis. This material is available free of charge via the Internet at http://pubs.acs.org.

REFERENCES

1. Blankenship, R. E., Madigan, M. T., and Bauer, C. E., Eds. (1995) *Anoxygenic Photosynthetic Bacteria*, Kluwer Academic Publishers, Dordrecht, The Netherlands.
2. Lin, X., Murchinson, H. A., Nagarajan, V., Parson, W. W., Allen, J. P., and Williams, J. C. (1994) Specific alteration of the oxidation potential of the electron donor in reaction centers from *Rhodobacter sphaeroides*, *Proc. Natl. Acad. Sci. U.S.A. 91*, 10265−10269.
3. Kálmán, L., LoBrutto, R., Allen, J. P., and Williams, J. C. (1999) Modified reaction centres oxidize tyrosine in reactions that mirror photosystem II, *Nature 402*, 696−699.
4. Kálmán, L., LoBrutto, R., Allen, J. P., and Williams, J. C. (2003) Manganese oxidation by modified reaction centers from *Rhodobacter sphaeroides*, *Biochemistry 42*, 11016−11022.
5. Hellinga, H. W. (1996) Metalloprotein design, *Curr. Opin. Biotechnol. 7*, 437−441.
6. Christianson, D. W. (1997) Structural chemistry and biology of manganese metalloenzymes, *Prog. Biophys. Mol. Biol. 67*, 217−252.
7. Ono, T. (2001) Metallo-radical hypothesis for photoassembly of $(Mn)_4$-cluster of photosynthetic oxygen evolving complex, *Biochim. Biophys. Acta 1503*, 40−51.
8. Debus, R. J. (2001) Amino acid residues that modulate the properties of tyrosine Y_Z and the manganese cluster in the water oxidizing complex of photosystem II, *Biochim. Biophys. Acta 1503*, 164−186.
9. Diner, B. A. (2001) Amino acid residues involved in the coordination and assembly of the manganese cluster of photosystem II. Proton-coupled electron transport of the redox-active tyrosines and its relationship to water oxidation, *Biochim. Biophys. Acta 1503*, 147−163.
10. Michel, H., and Deisenhofer, J. (1988) Relevance of the photosynthetic reaction center from purple bacteria to the structure of photosystem II, *Biochemistry 27*, 1−7.
11. Komiya, H., Yeates, T. O., Rees, D. C., Allen, J. P., and Feher, G. (1988) Structure of the reaction center from *Rhodobacter sphaeroides* R-26 and 2.4.1: Symmetry relations and sequence comparisons between different species, *Proc. Natl. Acad. Sci. U.S.A. 85*, 9012−9016.
12. Zouni, A., Witt, H. T., Kern, J., Fromme, P., Krauss, N., Saenger, W., and Orth, P. (2001) Crystal structure of photosystem II from *Synechococcus elongatus* at 3.8 Å resolution, *Nature 409*, 739−743.
13. Williams, J. C., Alden, R. G., Murchison, H. A., Peloquin, J. M., Woodbury, N. W., and Allen, J. P. (1992) Effects of mutations near the bacteriochlorophylls in reaction centers from *Rhodobacter sphaeroides*, *Biochemistry 31*, 11029−11037.
14. Williams, J. C., and Taguchi, A. K. W. (1995) Genetic Manipulation of Purple Photosynthetic Bacteria, in *Anoxygenic Photosynthetic Bacteria* (Blankenship, R. E., Madigan, M. T., and Bauer, C. E., Eds.) pp 1029−1065 Kluwer Academic Publishers, Dordrecht, The Netherlands.
15. Paddock, M. L., Rongey, S. H., Feher, G., and Okamura, M. Y. (1989) Pathway of proton transfer in bacterial reaction centers: Replacement of glutamic acid 212 in the L subunit by glutamine inhibits quinone (secondary acceptor) turnover, *Proc. Natl. Acad. Sci. U.S.A. 86*, 6602−6606.
16. Gerencsér, L., and Maróti, P. (2001) Retardation of proton transfer caused by binding of the transition metal ion to the bacterial reaction center is due to pK_a shifts of key protonatable residues, *Biochemistry 40*, 1850−1860.
17. Kleinherenbrink, F. A. M., Chiou, H. C., LoBrutto, R., and Blankenship, R. E. (1994) Spectroscopic evidence for the presence of an iron−sulfur center similar to FX of photosystem I in *Heliobacillus mobilis*, *Photosynth. Res. 41*, 115−123.
18. Allen, J. P., Feher, G., Yeates, T. O., Komiya, H., and Rees, D. C. (1987) Structure of the reaction center from *Rhodobacter sphaeroides* R-26: The cofactors, *Proc. Natl. Acad. Sci. U.S.A. 84*, 5730−5734.
19. Leslie, A. G. W. (1999) Integration of macromolecular diffraction data, *Acta Crystallogr. D55*, 1696−1702.
20. Cámara-Artigas, A., Brune, D., and Allen, J. P. (2002) Interactions between lipids and bacterial reaction centers determined by protein crystallography, *Proc. Natl. Acad. Sci. U.S.A. 99*, 11055−11060.
21. Collaborative Computational Project, Number 4 (1994) The CCP4 Suite: Programs for Protein Crystallography, *Acta Crystallogr. D50*, 760−763.
22. Brunger, A. T., and Rice, L. M. (1997) Crystallographic refinement by simulated annealing: Methods and applications, *Methods Enzymol. 277*, 243−269.
23. Kálmán, L., Narváez, A. J., LoBrutto, R., Williams, J. C., and Allen, J. P. (2004) Dependence of tyrosine oxidation in highly oxidizing bacterial reaction centers on pH and free-energy difference, *Biochemistry 43*, 12905−12912.
24. Page, C. C., Moser, C. C., Chen, X., and Dutton, P. L. (1999) Natural engineering principles of electron tunnelling in biological oxidation−reduction, *Nature 402*, 47−52.
25. Ferreira, K. N., Iverson, T. M., Maghlaoui, K., Barber, J., and Iwata, S. (2004) Architecture of the photosynthetic oxygen-evolving center, *Science 303*, 1831−1838.
26. Blankenship, R. E., and Hartman, H. (1998) The origin and evolution of oxygenic photosynthesis, *Trends Biochem. Sci. 23*, 94−97.
27. Johnson, E. T., and Parson, W. W. (2002) Electrostatic interactions in an integral membrane protein, *Biochemistry 41*, 6483−6494.
28. Widdel, F., Schnell, S., Heising, S., Ehrenreich, A., Assmus, B., and Schink, B. (1993) Ferrous iron oxidation by anoxygenic phototropic bacteria, *Nature 362*, 834−836.
29. Barker, P. D. (2003) Designing redox metalloproteins from bottom-up and top-down perspectives, *Curr. Opin. Struct. Biol. 13*, 490−499.

BI050377N